Rapid Communications | Editors' Suggestion

Higher-order acoustic phonon oscillations in Au nanoparticles controlled by a sequence of ultrashort strain pulses generated by superdiffusive hot electrons

Yooleemi Shin,[1,2,3] Yu Liu,[4] Mircea Vomir,[4] and Ji-Wan Kim[1,2,3,*]

[1]*Department of Physics, Kunsan National University, Kunsan 54150, South Korea*

[2]*Max Planck POSTECH/KOREA Research Initiative, Pohang 37673, South Korea*

[3]*Department of Physics and Center for Attosecond Science and Technology, POSTECH, Pohang 37673, South Korea*

[4]*Université de Strasbourg, CNRS, Institut de Physique et Chimie des Matériaux de Strasbourg, UMR 7504, Strasbourg 67034, France*

(Received 27 September 2019; revised manuscript received 27 November 2019; published 22 January 2020)

We demonstrate that higher-order acoustic phonon oscillations of self-assembled Au nanoparticles can be excited using higher frequency bandwidth picosecond acoustic pulses generated by superdiffusive hot electrons. These modes require directional excitations such as a longitudinal strain pulse, being inaccessible in a direct optical excitation scheme. They are detected using the periodic shift of the surface plasmon resonance and are coherently controlled by a sequence of delayed acoustic pulses. Acoustic mode calculations show that the high-frequency mode corresponds to two higher-order spheroidal modes.

DOI: 10.1103/PhysRevB.101.020302

The surface plasmon resonance (SPR), a well-known phenomenon - a strong electromagnetic interaction with matter [1], makes noble metallic nanostructures unique for many diverse applications such as photonic devices [2], single nanoparticle detection [3–5], biomedical [6–8] and chemical sensing [9]. During the last two decades, with the pursuit of faster control of optical properties, much attention has been focused on acoustic vibration eigenmodes excited by femtosecond optical pulses in confined nanostructures such as noble metal nanoparticles with well-defined shapes embedded in a matrix [10,11] and actively controlled patterned or superlattice nanostructures [12–17]. The absorption of the photon energy from optical pulses causes the subpicosecond change of the lattice parameter by a fast electron-lattice energy transfer and subsequent vibration motions leading to a strong periodic modification of SPR. The vibration eigenmodes reflect the optical properties of materials relevant to the size, shape, and environment of the nanostructures. However, when an optical pump pulse is used as the excitation source, the electron and lattice temperatures increase, resulting in a decrease of the absorption and a broadening of SPR [18]. This aspect makes the detailed quantification of the phonon vibration dynamics challenging. In contrast, a picosecond strain pulse is an excellent excitation source for surface plasmonic nanostructures since first, it can be well separated from the thermal energy depending on its travel distance and second, it has a high enough mechanical pressure of 0.1–1 GPa with a few picosecond temporal width to strongly modify the dimensions and properties of metallic systems. In that context, it has been recently shown that by using picosecond strain pulses as the excitation source, the angstrom dynamics of Au nanoparticles is precisely calculated without any assumption [19].

In this Rapid Communication, we have used ultrashort strain pulses to investigate acoustic vibration modes of Au nanoparticles (NPs) on Ni/Au films. The ultrashort strain pulses have been generated by superdiffusive hot electrons from an Au interlayer which shortens their duration by 1.9 times with respect to a direct optical excitation. The broader frequency bandwidth of thus generated acoustic pulses allows revealing the higher-order acoustic vibration spheroidal mode around 179 GHz otherwise not accessible by regular picosecond strain pulses. The higher-order mode is rigorously confirmed in the time domain by selectively suppressing the lowest-order mode using a two-pump coherent control experiment. The current results open standpoints for high-frequency nanoparticle dynamics toward the terahertz regime.

The spherical Au NP monolayer was prepared by the Langmuir-Blodgett assembly technique [20] on Ni (60 nm)/Au (300 nm) film deposited by magnetron sputtering on a sapphire substrate as shown in Fig. 1(a). A volume of a 5 mg/ml NP suspension in chloroform was spread on the water surface of the Langmuir-Blodgett trough. Au NPs were compressed by the mechanical barriers with a speed of 5 mm/min and the film was dipped and pulled vertically at a speed of 1 mm/min with reaching the maximum density of NPs onto the Ni/Au film area of 1×1 cm^2. More details of the sample preparation are described elsewhere [21]. The average radius of NPs is obtained from the transmission electron microscopy (TEM) image and the size distribution [Figs. 1(b) and 1(c)] to be $R_{\mathrm{Au}} = 5.2$ nm. The reflectance spectrum of Fig. 1(d) shows that the surface plasmon resonance is redshifted compared to that of a single Au nanoparticle, due to the interaction with both the dipole field from close-packed neighbors and the near field from Ni film underneath [19].

Figure 2(a) is the schematic diagram of our time-resolved two-pump–probe instrument. The experiment was performed by pumping the Au/sapphire interface with pump pulses (400 nm, 50 fs, $I = 2.0$ mJ/cm^2) and measuring the transient reflectivity $\Delta R(t)/R$ of Au NPs using s-polarized white-light

*Corresponding author: hwoarang.kim@gmail.com

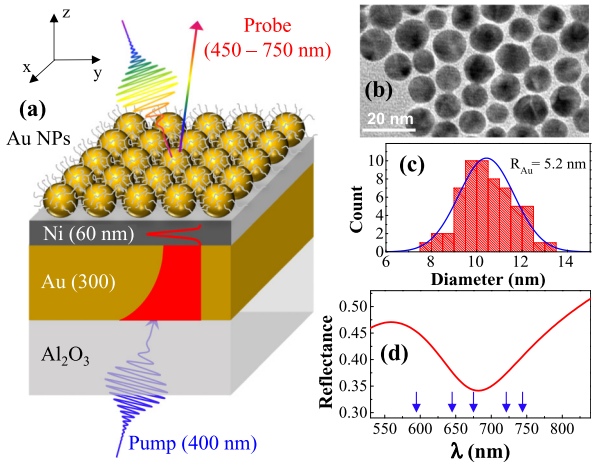

FIG. 1. (a) Sketch of the time-resolved strain pulse pump–continuum probe setup. Hot electrons generated at Au/Al_2O_3 interface by femtosecond pulses propagate superdiffusively to the Ni/Au interface and heat the Ni layer leading to the generation of the strain pulse. (b) TEM image of the self-assembled Au NP monolayer with a mean radius $R_{Au} = 5.2$ nm. (c) Histogram of Au NP size with Gaussian fit. (d) Static reflectance of the surface plasmon resonance band. The arrows correspond to the selected probe wavelengths for the time-resolved pump-probe experiments.

continuum probes (450–750 nm) generated from a sapphire plate. The role of the Au is to generate a shorter strain pulse [22]. When the pump pulses excite the Au film through the substrate, hot electrons are created through a transition from a flat d band to a sp-like band above the Fermi energy surface. The high electron mobility, due to the large curvature of the sp-like band, leads to a heat transport time of ∼300 fs to the Ni/Au interface [23,24]. When the hot electrons cross the interface, their energies are quickly redistributed by inelastic e-e scattering in Ni and thermally equilibrated by transferring their energies to the lattice with a stronger electron-phonon coupling than in Au [25,26]. This thermalization process results in a temperature increase of the Ni lattice and the thermal expansion of lattice triggers the strain pulse within a picosecond. Comparing with the standard way of generating picosecond strain pulses using a direct pump excitation [27–29], it is expected that the hot electrons generate shorter strain pulses as the absorption depth of hot electrons is shorter [24,30,31]. Figure 2(b) displays $\Delta R(t)$ of strain pulses for two samples probed with the fundamental wavelength of $\lambda =$ 800 nm: Ni (147 nm)/Al_2O_3 (red) and Ni (60 nm)/Au (300 nm)/Al_2O_3 (blue) without nanoparticles. The temporal width of the strain pulse profiles is obtained from the time derivatives of $\Delta R(t)$ as shown in Fig. 2(c) [32,33]. The temporal width of the ultrashort strain pulse induced by hot electrons is shorter by 1.9 times than that of the picosecond strain pulse. In a frequency domain, it is shown in Fig. 2(d) that the ultrashort strain pulse has a broader bandwidth by 1.4 times than that of the picosecond strain pulse.

Figure 3(a) shows $\Delta R(t)/R$ of Au NPs (solid circles) for five probe wavelengths ($\lambda_1 = 590$, $\lambda_2 = 640$, $\lambda_3 = 675$, $\lambda_4 =$ 720, and $\lambda_5 = 740$ nm), which are marked as vertical arrows

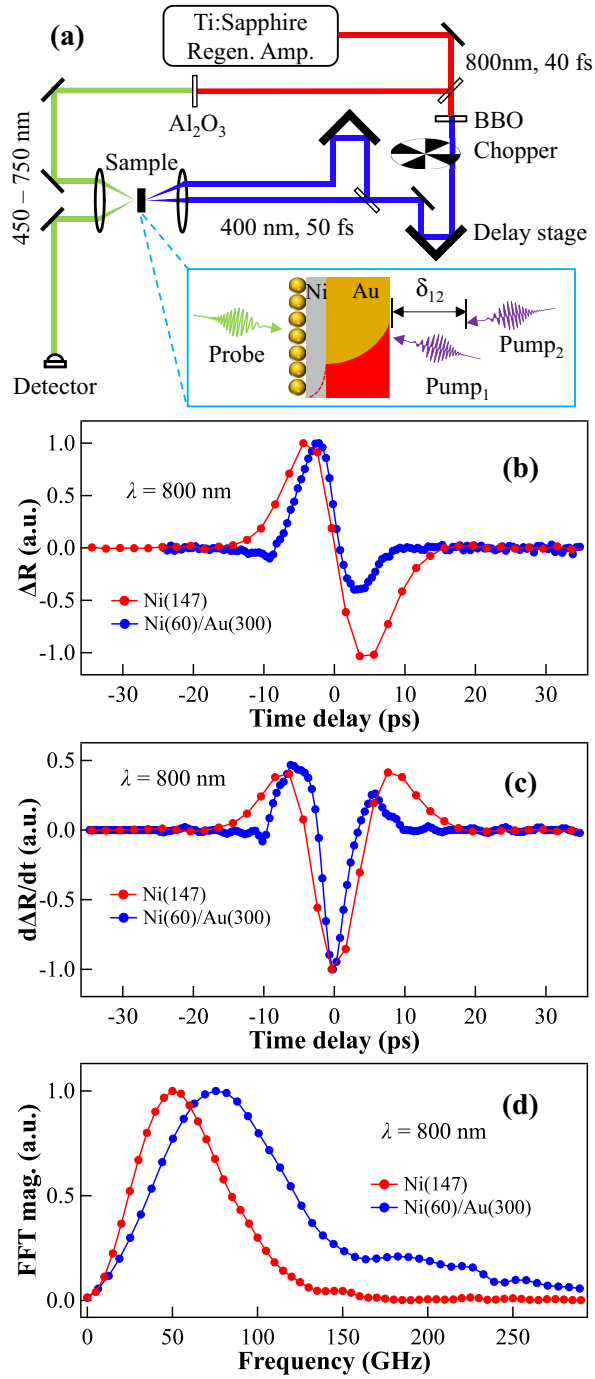

FIG. 2. (a) Schematic diagram of the time-resolved two-pump–probe instrument. Comparison of strain pulses for two samples, Ni/Al_2O_3 (red) and Ni/Au/Al_2O_3 (blue): (b) normalized $\Delta R(t)$, (c) normalized $d[\Delta R(t)]/dt$, and (d) FFT data of $d[\Delta R(t)]/dt$.

in Fig. 1(d) and $\Delta R(t)/R$ of the Ni film without Au NPs measured at λ_5 for the bottom curve (open circles). While the signals measured at the blue (λ_1, λ_2) and red (λ_4, λ_5) wings of the SPR show clear oscillations with opposite phase, the oscillations amplitude near the central wavelength of the resonance (λ_3) is much smaller. It is well known that the strain pulse changes both the real part $\varepsilon_r(\omega)$ and the imaginary part $\varepsilon_i(\omega)$ of the dielectric function [34,35] as it modifies the electronic

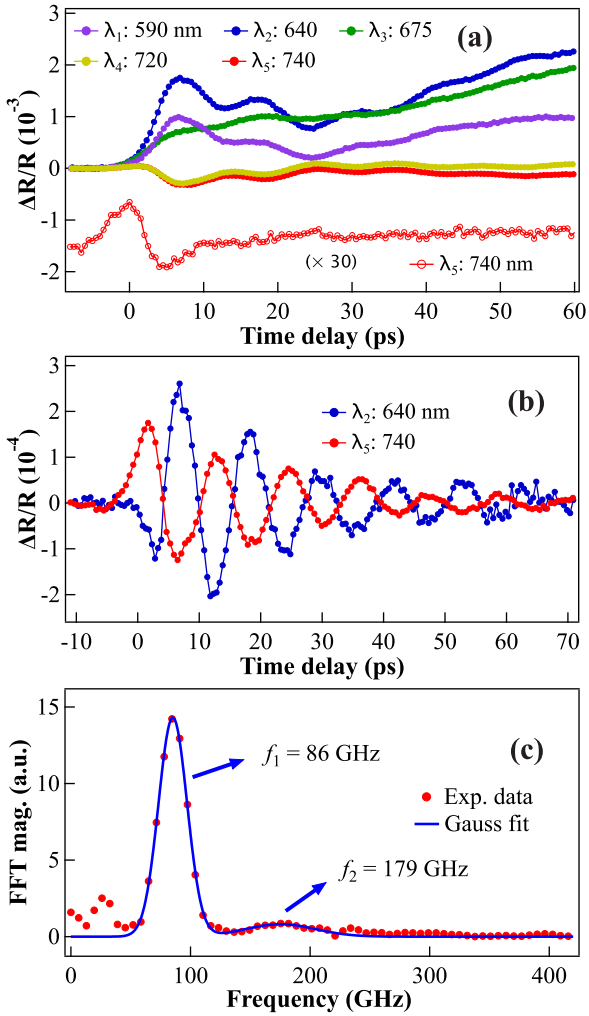

FIG. 3. (a) $\Delta R(t)/R$ of Au NPs (solid circles) for five probe wavelengths (λ_1: 590, λ_2: 640, λ_3: 675, λ_4: 720, and λ_5: 740 nm) selected in the vicinity of the surface plasmon resonance. For the timing reference, $\Delta R(t)/R$ of the strain pulse (without nanoparticles) probed at λ_5 is shown at the bottom. (b) $\Delta R(t)/R$ for two selected probe wavelengths (λ_2: blue; λ_5: red) after subtracting the background phonon signals. (c) FFT of $\Delta R(t)/R$ for λ_5 with Gaussian fits showing two vibration frequencies f_1, f_2.

band structure [36,37]. From the absorption function $\alpha(\omega)$ of a metal nanoparticle embedded in a dielectric medium $\alpha(\omega) = 4\pi\varepsilon_0 r^3(\varepsilon_{\rm Au} - \varepsilon_d)/(\varepsilon_{\rm Au} + 2\varepsilon_d)$, and the dielectric function of Au NPs

$$\varepsilon_{\rm Au} = \varepsilon_1 - \frac{\omega_p^2}{\omega^2 + i\Gamma(R_{\rm Au})\omega} + \frac{\varepsilon_2\omega_0^2}{\omega_0^2 - \omega^2 - 2i\delta_0\omega},$$

where ε_1, ε_2, and δ_0 are proper experimental values, ω_0 the resonance angular frequency, ω_p the plasma frequency, and $\Gamma(R_{\rm Au}) = \Gamma_{\rm bulk} + 1.3\upsilon_{\rm Fermi}/R_{\rm Au}$ the damping coefficient, it is easy to show that the change of $\varepsilon_{\rm Au}$, $\Delta\varepsilon_r(\omega) = \Delta\{-\omega_p^2/[\omega^2 + i\Gamma(R_{\rm Au})\omega]\}$ leads to a dynamical shift and broadening of the plasmon band. Therefore, if a particle size is changed periodically, a surface plasmon band would show the oscillatory behavior yielding an out-of-phase relation between $\Delta R(t)/R$ measured at opposite wings of the SPR, while the oscillation amplitude becomes almost zero at the center of the resonance as shown for λ_3 in Fig. 3(a). All parameter values used here can be found in Refs. [38,39].

The oscillatory behavior for λ_2 and λ_5 after subtracting the background signals corresponding to incoherent phonons and the axial phonon mode is shown in Fig. 3(b). When the compressive part of the strain pulse [$\Delta R(t)/R > 0$] arrives at the Au NPs/Ni interface, Au NPs are forced to be squeezed, i.e., a volume contraction (Poisson's ratio, $\nu_{\rm Au} = 0.44$) which leads to a blueshift of the SPR. It therefore induces first a negative sign of $\Delta R(t)/R$ for λ_2 and a positive sign for λ_5, respectively. A rough estimation gives the amount of the horizontal band shift in wavelength to be $\Delta\lambda_2 = (\frac{\Delta R(\lambda_2)}{R(\lambda_2)})\frac{R(\lambda_2)}{b(\lambda_2)} \sim 2.6 \times 10^{-4} \times \frac{0.39}{1.7\times10^{-3}} \sim 60$ pm, where $b(\lambda)$ stands for the reflectance slope at a given λ. For a closer look into the acoustic phonon eigenmodes, the fast Fourier transform (FFT) of $\Delta R(t)/R$ for λ_5 is displayed in Fig. 3(c) with its corresponding Gaussian fitting. The low (f_1) and high (f_2) frequencies are assigned to 86 and 179 GHz, respectively. We stress that the maximum frequency of the eigenmode that can be excited is determined by the frequency bandwidth of the excitation source. In this experiment, the frequency bandwidth of the strain pulse generated by hot electrons slightly covers the f_2 frequency, while the strain pulse induced by direct laser pump excitation does not.

In a previous study, we have shown that the f_1 mode corresponds to a periodic volume contraction and elongation of NPs, which corresponds to the quadrupole mode $(n, l) = (0, 2)$ (n, the harmonic order, i.e., the number of radial nodes inside the sphere and l, the angular quantum number) [19]. To focus on the high-frequency f_2 mode only, which is rarely distinct in the time domain, we performed a two-pump experiment ($I_1 = I_2 = I/2$) with time delay δ_{12} between the two pump pulses. Here, the second pump acts as a control pulse to coherently amplify or suppress a given mode for an appropriate delay δ_{12} [40,41]. The FFT data in Fig. 4(a) show that the two phonon modes are well controlled using two pumps. For $\delta_{12} = 1/2f_2 \sim 2.8$ ps, the f_2 mode is suppressed (red) while for $\delta_{12} = 1/2f_1 \sim 5.5$ ps, the f_1 mode is suppressed and the f_2 mode becomes comparatively contrasted (blue). For the wide range of $-0.5 \leqslant \delta_{12} \leqslant 8$ ps with a step of ~0.4 ps, we present the two-dimensional mapping of FFT in the inset. The two dashed horizontal lines correspond to $\delta_{12} = 2.8$ and 5.5 ps. To make a better contrast of f_2, we multiplied by a factor of 5 the FFT magnitude in the region of $f > 118$ GHz (marked as a dashed vertical line). As shown in Fig. 4(b), after subtracting the phonon background signals for $\delta_{12} = 5.5$ ps, the f_2 mode is clearly distinguished in the time domain. Its amplitude corresponds to ~6 pm plasmon band shift in wavelength.

To identify the f_2 mode in the confined nanoparticle structure, we calculate the acoustic eigenmodes of a solid elastic sphere based on Lamb's theory. Under the conditions of a stress-free boundary (no embedding matrix) and a homogeneous spherical elastic medium, the equation of motion in a

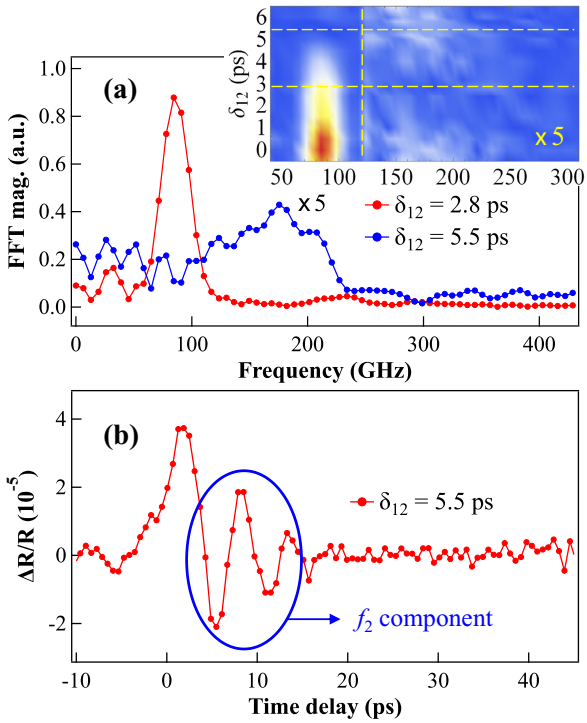

FIG. 4. (a) Selection of acoustic modes using the coherent control with two pump pulses delayed by a time δ_{12}. (a) FFT data for $\delta_{12} = 2.8$ (red, f_2 suppression) and 5.5 ps (blue, f_1 suppression), respectively. In the inset, two-dimensional mapping of FFT for $-0.5 \leqslant \delta_{12} \leqslant 8$ ps is shown. To give the f_2 mode a better contrast, the magnitude in the region of $f > 118$ GHz (marked as a dashed vertical line) is multiplied by a factor of 5. (b) f_2 mode in the time domain obtained for $\delta_{12} = 5.5$ ps.

spherical coordinate is derived as follows [42,43]:

$$\xi_{nl} j_0(\xi_{nl}) - 4\left(\frac{\upsilon_T}{\upsilon_L}\right)^2 j_1(\xi_{nl}) = 0, \quad l = 0,$$

$$\left\{1 + \frac{(l-1)(l+2)}{\eta^2}\left[J_l^{l+1}(\eta) - (l+1)\right]\right\} 2J_l^{l+1}(\xi)$$

$$+\left\{1 - \frac{2l(l-1)(l+2)}{\eta^2}\right\} J_l^{l+1}(\eta)$$

$$+(l-1)(2l+1) - \frac{\eta^2}{2} = 0, \quad l \geqslant 1,$$

where j_l is the spherical Bessel function; $J_l^{l+1}(m) = j_{l+1}(m)/j_l(m)$; $\upsilon_L = 3240$ and $\upsilon_T = 1200$ m/s are the longitudinal and transverse speed of sound; $\xi_{nl} = h_{nl,L}R$, $\eta_{nl} = h_{nl,T}R$, $h_{nl,L} = 2\pi f_{nl}/\upsilon_L$, and $h_{nl,T} = 2\pi f_{nl}/\upsilon_T$, respectively. In our experimental conditions, the fundamental breathing and its harmonic modes $(n, l = 0)$ are not observed since the strain pulse excitation is not radially isotropic. For the f_2 mode, the above equation gives two possible eigenmode frequencies: $(n, l) = (0, 4)$ [44], $f_{04} = 186$ GHz and $(n, l) = (1, 2)$, $f_{12} = 192$ GHz. The slight difference between the experimental f_2 value and that from calculations may find its origin in the decrease of elastic stiffness of Au NPs, which is directly related to υ_L and υ_T, due to the influence of grain boundaries and dislocations [45,46]. In addition, adjoining NPs as appeared in Fig. 1(b) lower the mode frequencies due to the effect of larger NP size. However, it is hard to determine without ambiguity which mode corresponds to f_2 since $(0, 4)$ and $(1, 2)$ spheroidal mode frequencies are too close to be resolved in our experimental configuration. It can be fairly thought that the quadrupole harmonic mode $(1, 2)$ is rarely detected because of the smaller volume change by one radial node inside. Nevertheless, since this mode is not forbidden by considering the axial excitation symmetry, the two spheroidal modes can exist simultaneously. To resolve this small frequency difference between the two modes, more accurate measurements should be carried out with better sample characteristics such as monodisperse and larger size of nanoparticles, a perfect spherical shape and crystalline structure, a homogeneous elastic property, and a low plasmon damping taking into account the interface [47]. Moreover, we found that the 235 GHz signal at $\delta_{12} = 2.8$ ps in Fig. 4(a) is coherently controlled by the two-pump experiment and the frequency may correspond to the $(0, 6)$ spheroidal mode as shown by the elastic sphere calculations. However, one should be careful to assign it due to its small signal-to-noise ratio in the frequency domain and due to the absence of a clear disentanglement in the time domain (not shown here).

In conclusion, we have demonstrated that the picosecond strain pulses, generated by hot electrons, excite efficiently acoustic phonon eigenmodes in Au nanoparticles. The volume modulation caused by acoustic modes leads to a periodic change in the free electron density, which induces a periodic shift (as small as few tens of picometers) of the surface plasmon band. In contrast to the direct laser pump excitation for strain pulse generation, it has been proved that hot electrons generate shorter strain pulses. They allow revealing high-frequency acoustic phonon modes apart from the lowest-order quadrupole mode $(0, 2)$ that has been previously observed. A coherent control of the phonon modes using a two-pump experiment clearly identifies in the time domain the high-frequency mode (179 GHz) by completely suppressing the $(0, 2)$ mode. Although the high-frequency mode is hard to be clearly assigned in this experiment due to the broadness of the peak in the frequency domain, the solid elastic sphere calculation suggests both the $(1, 2)$ and $(0, 4)$ spheroidal modes, which are new observed modes in our size of the Au nanoparticle that cannot be active with a direct optical pumping. Importantly, we also note that the picosecond strain pulse excluding transient optical bleaching makes this method suitable for revealing new acoustic modes with extreme sensitivity.

This work was supported by Basic Science Research Program through the National Research Foundation of Korea (NRF) funded by the Ministry of Education (2017R1A6A3A04011173 and 2017R1A6A3A11032995), and by Korea Institute for Advancement of Technology (KIAT) grant funded by the Korea Government (MOTIE) (P0008763, The Competency Development Program for Industry Specialist), and by Max Planck POSTECH/KOREA Research Initiative Program (Grant No. 2016K1A4A4A01922028) through the National Research

Foundation of Korea (NRF) funded by Ministry of Science, ICT and Future Planning, and by the Agence Nationale de la Recherche in France via the project EquipEx UNION No. ANR-10-EQPX-52.

[1] S. A. Maier, *Plasmonics: Fundamentals and Applications* (Springer Science & Business Media, Berlin, 2007).
[2] W. L. Barnes, A. Dereux, and T. W. Ebbesen, Nature (London) **424**, 824 (2003).
[3] S. A. Maier, P. G. Kik, H. A. Atwater, S. Meltzer, E. Harel, B. E. Koel, and A. A. Requicha, Nat. Mater. **2**, 229 (2003).
[4] M. A. van Dijk, M. Lippitz, and M. Orrit, Phys. Rev. Lett. **95**, 267406 (2005).
[5] P. V. Ruijgrok, P. Zijlstra, A. L. Tchebotareva, and M. Orrit, Nano Lett. **12**, 1063 (2012).
[6] A. J. Haes, W. P. Hall, L. Chang, W. L. Klein, and R. P. Van Duyne, Nano Lett. **4**, 1029 (2004).
[7] M. Holzinger, A. Le Goff, and S. Cosnier, Front. Chem. **2**, 63 (2014).
[8] J. Cheng, E. H. Hill, Y. Zheng, T. He, and Y. Liu, Mater. Chem. Front. **2**, 662 (2018).
[9] A. Chen and S. Chatterjee, Chem. Soc. Rev. **42**, 5425 (2013).
[10] M. Hu, X. Wang, G. V. Hartland, P. Mulvaney, J. P. Juste, and J. E. Sader, J. Am. Chem. Soc. **125**, 14925 (2003).
[11] D. Mongin, P. Maioli, J. Burgin, P. Langot, E. Cottancin, S. D'Addato, B. Canut, M. Treguer, A. Crut, F. Vallée, and N. Del Fatti, J. Phys.: Condens. Matter **31**, 084001 (2019).
[12] V. V. Temnov, Nat. Photonics **6**, 728 (2012).
[13] K. O'Brien, N. Lanzillotti-Kimura, J. Rho, H. Suchowski, X. Yin, and X. Zhang, Nat. Commun. **5**, 4042 (2014).
[14] C. Yi, P. D. Dongare, M.-N. Su, W. Wang, D. Chakraborty, F. Wen, W.-S. Chang, J. E. Sader, P. Nordlander, N. J. Halas *et al.*, Proc. Natl. Acad. Sci. USA **114**, 11621 (2017).
[15] J. Wang, K. Yu, Y. Yang, G. V. Hartland, J. E. Sader, and G. P. Wang, Nat. Commun. **10**, 1527 (2019).
[16] T. Schumacher, K. Kratzer, D. Molnar, M. Hentschel, H. Giessen, and M. Lippitz, Nat. Commun. **2**, 333 (2011).
[17] P. Ruello, A. Ayouch, G. Vaudel, T. Pezeril, N. Delorme, S. Sato, K. Kimura, and V. E. Gusev, Phys. Rev. B **92**, 174304 (2015).
[18] S. Link, C. Burda, Z. L. Wang, and M. A. El-Sayed, J. Chem. Phys. **111**, 1255 (1999).
[19] J.-W. Kim, O. Kovalenko, Y. Liu, and J.-Y. Bigot, ACS Nano **10**, 10880 (2016).
[20] A. Tao, F. Kim, C. Hess, J. Goldberger, R. He, Y. Sun, Y. Xia, and P. Yang, Nano Lett. **3**, 1229 (2003).
[21] Y. Liu, S. Begin-Colin, B. P. Pichon, C. Leuvrey, D. Ihiawakrim, M. Rastei, G. Schmerber, M. Vomir, and J. Y. Bigot, Nanoscale **6**, 12080 (2014).
[22] V. Shalagatskyi, O. Kovalenko, V. Shumylo, A. Alekhin, G. Vaudel, T. Pezeril, V. S. Vlasov, A. M. Lomonosov, V. E. Gusev, D. Makarov, and V. V. Temnov, arXiv:1511.09060.
[23] S. D. Brorson, J. G. Fujimoto, and E. P. Ippen, Phys. Rev. Lett. **59**, 1962 (1987).
[24] M. Lejman, V. Shalagatskyi, O. Kovalenko, T. Pezeril, V. V. Temnov, and P. Ruello, J. Opt. Soc. Am. B **31**, 282 (2014).
[25] Z. Lin, L. V. Zhigilei, and V. Celli, Phys. Rev. B **77**, 075133 (2008).
[26] M. Battiato, K. Carva, and P. M. Oppeneer, Phys. Rev. Lett. **105**, 027203 (2010).
[27] T. Saito, O. Matsuda, and O. B. Wright, Phys. Rev. B **67**, 205421 (2003).
[28] A. V. Scherbakov, A. S. Salasyuk, A. V. Akimov, X. Liu, M. Bombeck, C. Brüggemann, D. R. Yakovlev, V. F. Sapega, J. K. Furdyna, and M. Bayer, Phys. Rev. Lett. **105**, 117204 (2010).
[29] J.-W. Kim, M. Vomir, and J.-Y. Bigot, Phys. Rev. Lett. **109**, 166601 (2012).
[30] G. Tas and H. J. Maris, Phys. Rev. B **49**, 15046 (1994).
[31] M. Bonn, D. N. Denzler, S. Funk, M. Wolf, S.-Svante Wellershoff, and J. Hohlfeld, Phys. Rev. B **61**, 1101 (2000).
[32] K. J. Manke, A. A. Maznev, C. Klieber, V. Shalagatskyi, V. V. Temnov, D. Makarov, S.-H. Baek, C.-B. Eom, and K. A. Nelson, Appl. Phys. Lett. **103**, 173104 (2013).
[33] V. V. Temnov, C. Klieber, K. A. Nelson, T. Thomay, V. Knittel, A. Leitenstorfer, D. Makarov, M. Albrecht, and R. Bratschitsch, Nat. Commun. **4**, 1468 (2013).
[34] M. Garfinkel, J. J. Tiemann, and W. E. Engeler, Phys. Rev. **148**, 695 (1966).
[35] U. Gerhardt, Phys. Rev. **172**, 651 (1968).
[36] P. Etchegoin, J. Kircher, M. Cardona, and C. Grein, Phys. Rev. B **45**, 11721 (1992).
[37] A. V. Akimov, A. V. Scherbakov, D. R. Yakovlev, C. T. Foxon, and M. Bayer, Phys. Rev. Lett. **97**, 037401 (2006).
[38] N. C. Dyck, R. C. Denomme, and P. M. Nieva, J. Phys. Chem. C **115**, 15225 (2011).
[39] P. B. Johnson and R.-W. Christy, Phys. Rev. B **6**, 4370 (1972).
[40] C. Voisin, N. Del Fatti, D. Christofilos, and F. Vallée, J. Phys. Chem. B **105**, 2264 (2001).
[41] A. Arbouet, N. Del Fatti, and F. Vallee, J. Chem. Phys. **124**, 144701 (2006).
[42] N. Nishiguchi and T. Sakuma, Solid State Commun. **38**, 1073 (1981).
[43] P. Verma, W. Cordts, G. Irmer, and J. Monecke, Phys. Rev. B **60**, 5778 (1999).
[44] T. Dehoux, T. A. Kelf, M. Tomoda, O. Matsuda, O. B. Wright, K. Ueno, Y. Nishijima, S. Juodkazis, H. Misawa, V. Tournat, and V. E. Gusev, Opt. Lett. **34**, 3740 (2009).
[45] J. Schiøtz, T. Vegge, F. D. Di Tolla, and K. W. Jacobsen, Phys. Rev. B **60**, 11971 (1999).
[46] T. D. Shen, C. C. Koch, T. Y. Tsui, and G. M. Pharr, J. Mater. Res. **10**, 2892 (1995).
[47] B. Foerster, V. A. Spata, E. A. Carter, C. Sönnichsen, and S. Link, Sci. Adv. **5**, eaav0704 (2019).